# A single-ossicle ear : acoustic response and mechanical properties measured in duck

# A single-ossicle ear: acoustic response and mechanical properties measured in duck

Pieter G.G. Muyshondt[a,1], Joris A.M. Soons[a], Daniël De Greef[a], Felipe Pires[ab], Peter Aerts[c], Joris J.J. Dirckx[a]

[a]*Laboratory of Biophysics and Biomedical Physics, University of Antwerp, Groenenborgerlaan 121, 2020 Antwerp, Belgium*
[b]*Department of Mechanical Engineering, Free University of Brussels, Pleinlaan 2, 1050 Brussels*
[c]*Functional Morphology, University of Antwerp, Universiteitsplein 1, 2610 Antwerp, Belgium*
[1]*E-mail address: pieter.muyshondt@uantwerpen.be*

## Abstract

To date, the single-ossicle avian middle ear (ME) is poorly understood, despite its striking resemblance to the design of many currently used ossicular replacement prostheses. This study aims to improve comprehension of this system. The acoustic response and the mechanical properties of the mallard middle ear were studied by means of optical interferometry experiments and finite element (FE) simulations. A finite element model was constructed based on μCT data and validated using the experimental results. Stroboscopic holography was used to measure the full-field displacement of the tympanic membrane (TM) under acoustic stimulation, and the transfer function was obtained with laser Doppler vibrometry. A sensitivity analysis concluded that the most influential parameters for ME mechanics are the elasticity of the TM, the extracolumella (the cartilaginous part of the columella) and the annular ligament of the columellar footplate. Estimates for the Young's modulus of the TM were obtained by iteratively updating the FE model to match experimental data. A considerable inter-individual variability was found for the TM's elasticity. Comparison of the experimental results and the optimized FE model shows that, similar to the human middle ear, damping needs to be present in the TM to describe the specific spatial and frequency dependent vibrations of the TM. In summary, our results indicate which mechanical parameters are essential to the good functioning of the avian ME and provide a first estimation of their values.

## Keywords

Avian middle ear, stroboscopic holography, laser vibrometry, finite element modeling, model optimization.

## Highlights

- ME mechanics were studied in duck by holography, vibrometry and FE modeling,
- A sensitivity analysis was done to determine the influence of material parameters,
- The Young's modulus of the TM was estimated in inverse analysis on three specimens,
- Internal damping must be present in the TM to describe the experimental results.

## Abbreviations

| | |
|---|---|
| (μ)CT | (micro) computed tomography |
| AL | annular ligament |
| C | columella |
| ES | extrastapedial process |
| EST | extrastapedial tip |
| EXC | extracolumella |
| FE | finite element |
| FP | footplate |
| IE | inner ear |
| IS | infrastapedial process |
| MDT | middle drum-tubal ligament |

| | |
|---|---|
| ME | middle ear |
| S1,2,3 | sample 1, 2 or 3 |
| SPL | sound pressure level |
| SS | suprastapedial process |
| ST | soft tissue structures |
| TM | tympanic membrane |

## 1. Introduction

The avian middle ear (ME) uses the tympanic membrane (TM), a cartilaginous unit (the extracolumella) (EXC) and a single ossicle (the columella) to bridge the acoustic impedance difference between air and the fluids of the inner ear (IE). Although the hearing frequency range in birds is generally smaller than in mammals, with an upper frequency limit around roughly 10 kHz (Dooling et al., 2002), hearing thresholds in both classes are mostly comparable. Just as in mammals, impedance matching in avian species is obtained by three mechanisms: (1) a hydroacoustic transformation represented by the TM-to-footplate area ratio, (2) a mechanical lever action based on rotations around a fulcrum (Saunders et al., 2002), and (3) a curved membrane effect. The mechanical lever is supposed to go along with a tilting motion of the columella and the footplate (FP), given the acute angle between the ossicle and the TM plane (Gaudin, 1968), although detailed measurements are missing. A piston-like motion has been reported in one owl species, which was attributed to an additional flexing motion of the EXC (Norberg, 1978).

It is not well understood how the avian ME deals with quasi-static pressure changes. It has been suggested that the intracolumellar joint plays a role by performing a buckling motion, which is identified as a synchondrosis that functions as a ball joint (Mills and Zhang, 2006; Arechvo et al., 2013). To understand this quasi-static and acoustic behavior, a thorough knowledge is needed of the mechanical parameters that describe the columellar bird ear. Understanding the functioning of the single-ossicle avian ear may eventually contribute to the improvement of current single-ossicle prosthesis.

Studies of the mechanical properties of the avian ME are scarce, and only describe (quasi-)static characteristics (e.g. Thomassen et al., 2007). Moreover, a priori knowledge of material parameters is lacking entirely. In this study, the acoustic response and mechanical properties were investigated in mallard duck (*Anas platyrhynchos*) by meatns of optical interferometry and finite element (FE) modeling. Sound-induced motions of the TM were measured with stroboscopic holography to obtain its full-field displacement, and the sound-induced velocities of the columellar footplate and the conical tip of the TM were measured using a laser Doppler vibrometer. A 3D FE model of a duck's ME is constructed, based on the geometry obtained from μCT scans. Using this model, the mechanics of the ME are simulated under acoustic stimulation of the TM. Since initially defined material parameters are uncertain, a sensitivity analysis is performed to quantify their relative influence on the model output. Afterwards, the most influential parameter is determined in inverse analysis for different specimens, which allows us to study the acoustic behavior and viscoelastic properties of the TM at multiple frequencies.

## 2. Methods

### *2.1 Experiments*

#### *2.1.1 Sample preparation*

Measurements were performed on three dissected left ears of defrosted mallard duck heads (S1, S2 and S3). S1 and S2 were male and S3 female. Under the operation microscope, no signs of pathology were detected. During preparation, a part of the left side of the skull containing the ME was dissected from the head, which opened the bilaterally connected middle-ear cavities. The quadrate, which is a part of the beak suspension connected to the ME, was partially removed and the major part of the ear canal was drilled away to expose the TM. After a first set of measurements, the IE load on the ME was removed by drilling away its medial wall and draining the IE fluid. The samples were kept moist by use of a vaporizer (Bionaire) and by putting them in hydrated paper between the preparation and the measurements. In between measurements, samples were stored in refrigerated saline solution.

### 2.1.2 Stroboscopic holography

Digital stroboscopic holography enables the quantitative measurement of full-field displacement of a vibrating object as a function of time. This is realized by synchronizing very short laser pulses (8 ns) to the vibration phase so that the object's motion is 'frozen in time'. The full-field displacement at the chosen phase is then calculated by comparing the displaced hologram to a reference hologram of the object in rest. By cycling the laser pulses stepwise through the vibration period at evenly-spaced phase instants, the entire time-resolved transverse motion of the surface is obtained. After Fourier analysis of the time-dependent displacement waveforms, the displacement magnitude and phase maps can be obtained. The exact phase difference between the incident sound waves and the vibrating surface is monitored with an oscilloscope. For a more detailed description of this technique, see Cheng et al. (2010, 2013), Khaleghi et al. (2013) and De Greef et al. (2014a). Sound pressures of 11 frequencies ranging from 0.05 to 12.8 kHz, two per octave, were applied to the lateral side of the TM with pressure amplitudes between 90 and 110 dB SPL. The actual sound pressure at the TM was recorded with a probe microphone. During the measurement, the samples were placed inside a fixture with the TM plane positioned perpendicular to the illumination beam of the laser. On S3, the motion was measured with both intact and removed IE to measure the effect of the IE impedance on the TM response. To enhance reflectivity of the TM, the membrane was painted with a thin layer of either of two different coatings: a suspension of 5% TiO2 in deionized water for S1 and white make-up liquid (Kryolan Aquacolor Soft Cream - White Wet Make-up, Product Code 01129/00; Kryolan, Berlin, Germany) for S2 and S3. Tests showed that the latter gives the best combination of reflectivity, ease of application and delay of dehydration.

### 2.1.3 Laser Doppler vibrometry

The sound-induced motions of the ossicle were measured on S2 and S3 using a laser Doppler vibrometer (OFV-534, Polytec, Waldbronn, Germany) that is mounted on a surgical microscope (OPMI Sensera/S7, Carl Zeiss, Jena, Germany). Sound-induced velocities were divided by the sound pressure measured in front of the TM to define the middle-ear transfer functions. To enhance reflectivity, a little piece of reflective tape is placed onto the point of measurement, small enough to minimize inertial effects. During measurement, the laser beam was pointed perpendicular to the object's surface. Pure tone sinusoidal pressures, 16 per octave, with amplitudes of 90 dB were presented to the lateral TM surface. A probe microphone was placed in front of the TM to measure the actual pressure. Experiment control and signal processing was done in Matlab. Since it was not feasible to have optical access to the footplate from the lateral side, the following approach was applied: first, the velocity response was measured at the conical tip of the TM from the lateral side, with IE intact. Then, the IE was opened and drained and the transfer function was measured again at the TM to examine the effect of the IE impedance. Finally, the response was measured at the FP in the oval window from the medial side.

## 2.2 Finite element modeling

### 2.2.1 Morphology

The geometry for our FE model is based on µCT images of a dissected left ear of a mallard duck, different from the ones used in the experiments. The µCT scan was executed at the University of Ghent Computer Tomography (UGCT) facility (Masschaele et al., 2007). To enhance soft tissue contrast, the ME sample was stained during two days before scanning using a daily refreshed 2.5% PTA solution in deionized water, which limits tissue shrinkage most (Buytaert et al., 2014). The resulting dataset is built up of 2000x2000x1640 cubic voxels with a voxel size of 7.5 µm. Image segmentation of the CT data was carried out in Amira® 5.3 (FEI Visualization Sciences Group, Hillsboro, Oregon, USA). An automatic seed fill algorithm was applied together with an interpolation method to obtain the segmentation, although manual intervention was required to detect boundaries of soft tissue structures. After segmentation the different geometric components were converted separately into triangulated surface objects (STL), which were recombined in FE software (COMSOL® Multiphysics 5.0, Burlington, Massachusetts, USA). The final triangulated surface contains the ME structures shown in Fig. 1, but the ear canal, the ME cavity wall and the IE were not considered, in order to not overcomplicate the model and

to obtain well-defined boundary conditions. The geometry includes the following objects: a slightly conical TM with the apex pointing outwards into the ear canal, the columella bounded by an annular ligament, the EXC considered as a single unit comprising three arms (the infra-, extra- and suprastapedial processes), and Platner's ligament made of collagen fibers which extends across the ME cavity onto the otic process of the quadrate (Starck, 1995). The extrastapedial process ends in the apex of the conical TM which is referred to as the extrastapedial tip (EST). The ratio of the TM-to-FP surface area equals 23.2 and the columella is tilted 59.6° relative to the TM plane. Several ligaments and muscles mentioned in literature (Pohlman, 1921) were not apparent in the scan and were not considered in the final geometry. This includes the columellar muscle which inserts onto the columella, the drum-tubal ligaments that run through the TM, and the ascending ligament which connects the TM to the extrastapedial process and is comparable to the manubrial fold in mammals.

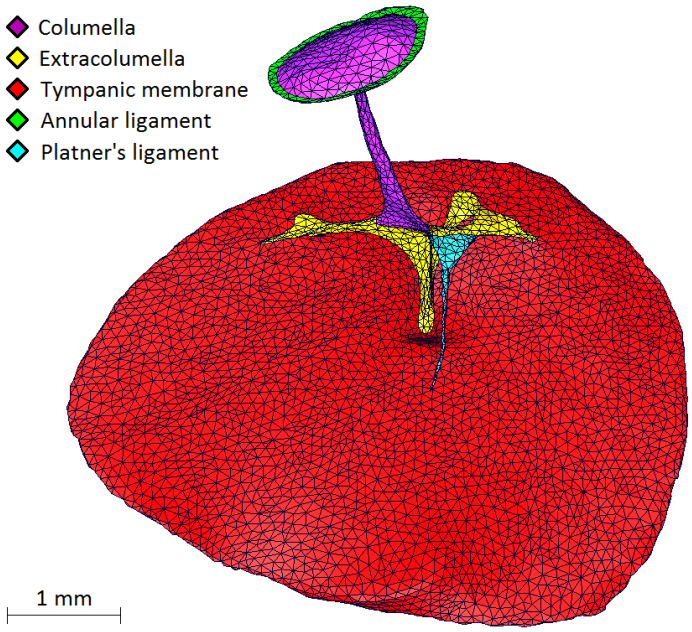


**Figure 1.** Triangulated surface model of the left ME of a mallard duck. All different components are indicated in color.

### *2.2.2 Model description and boundary conditions*

In the FE mesh, the TM is described as a 2D shell structure and was meshed using triangular elements. To take into account the non-uniform thickness distribution of the TM, the original segmentation data was used to calculate the full-field thickness of the membrane by adaptation of Van der Jeught et al. (2013), which is defined as the perpendicular distance from the medial to the lateral TM plane, as depicted in Fig. 2. Platner's ligament was modeled by triangular shell elements near the connection with the EXC, and by 1D beam elements along the length of the ligament, having uniform thickness and diameter as calculated from the segmentation data. The shaft of the bony columella and the cartilaginous EXC are meshed using 3D tetrahedral solid elements. For the FP and annular ligament shell elements were used, with non-uniform thickness distribution as shown in Fig. 2. Adjacent solid and shell objects are rigidly connected, which means that shared nodes yield equal displacements, also at the intracolumellar joint. In addition, beam-shell connections share rotational degrees of freedom. As a boundary condition, the outer rim of the TM and the annular ligament are fully constrained, allowing neither rotations nor displacements. Also, Platner's ligament is fully constrained at the border with the quadrate. At the medial surface of the FP, a viscoelastic load was applied to model the impedance of IE fluids, with a total spring constant of 525.8 N/m and damping coefficient of 0.771 N·s/m, adapted from Merchant et al. (1996). Modeling was done in the frequency domain to calculate the steady-state response of the entire geometry at individual frequencies. To simulate the acoustic stimulus of the TM, a uniform harmonic pressure of 1 Pa (i.e. 94 dB SPL) was applied at the lateral TM surface.

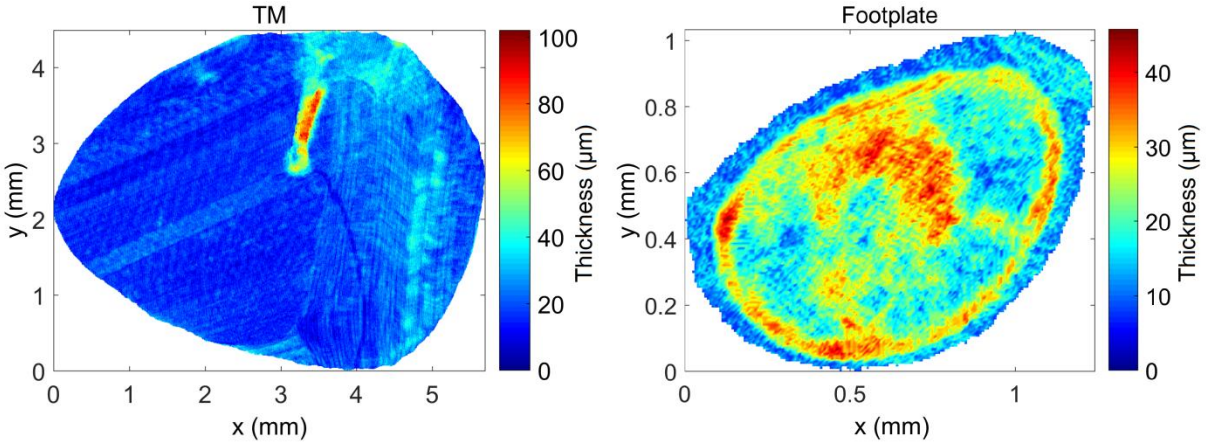


**Figure 2**. Thickness distributions of the TM (left) and FP (right). The TM thickness is largest near the attachment of the extrastapedial process of the EXC, which corresponds to the location of the ascending ligament. The FP thickness is largest around the connection with the annular ligament.

### *2.2.3 Material properties*

All objects made of soft tissue were treated as viscoelastic materials. Only the bony columella was treated as a purely elastic material. Viscoelasticity in the frequency domain was modeled by a complex modulus $E'$ defined as

$$E'(\omega) = E_1(\omega) + iE_2(\omega) = E_1(\omega)[1 + i\eta(\omega)], \quad (1)$$

in which $\omega$ represents the angular frequency, $i$ the imaginary unit, $E_1$ the storage or Young's modulus (unit: Pa, further on assigned by $E$) that accounts for the elastic part, $E_2$ the loss modulus that takes into account the viscous portion (unit: Pa), and $\eta = E_2/E_1$ the loss factor, which is a dimensionless quantity equal to zero for purely elastic materials. Since no avian ME parameters are available, they were initially taken from other literature values, which are given in Table 1, all considered homogeneous and isotropic.

| Component | $\rho$ ($10^3$ kg/m$^3$) | $E$ (MPa) | $\eta$ | $v$ |
|---|---|---|---|---|
| Columella | 2.2 | 14100[a] | 0 | 0.3 |
| EXC | 1.2 | 39.2[b] | 0.078[d] | 0.3 |
| TM | 1.2 | 20[a] | 0.078[d] | 0.3 |
| Platner's lig. | 1.2 | 21[c] | 0.078[d] | 0.3 |
| Annular lig. | 1.2 | 20[e] | 0.078[d] | 0.3 |

**Table 1.** Material parameter values used in the initial FE model. All mass densities $\rho$, Poisson's ratios $v$, and values indicated with [a] are taken from (Homma et al. 2010), being frequently used in current human ME models.[b] is taken from (Spahn and Wittig, 2003) which is based on hyaline cartilage values in the knee of a domestic pig.[c] is taken from (Homma et al., 2009) and comes from values of the human anterior mallear ligament.[d] is taken from (Aernouts et al., 2012) and represents a constant loss factor derived for the human TM, here used for all soft tissue structures.[e] is taken from (Thomassen et al., 2007) and was used to model the annular ligament in birds that consists of collagen.

To describe the frequency dependence of the viscoelastic TM, three model descriptions were applied that were used in De Greef et al. (2014b). **Model 1**: constant values for $E$ and $\eta$ for the TM, given in Table 1. **Model 2**: a third order generalized Maxwell model, comprised of a spring in parallel with three spring-dashpots in series with frequency dependent storage and loss moduli (Zhang and Gan, 2010). **Model 3**: A Rayleigh damping model with frequency dependent loss factor (Volandri et al., 2011) and constant Young's modulus.

### *2.2.4 Inverse analysis*

Since no a priori knowledge is available of the avian ME parameters, there is a considerable uncertainty on the initial values defined in Table 1. To characterize which parameters have the largest influence on the model

output, a sensitivity analysis was performed using the technique of Oakley and O'Hagan (2004). The values for two most influential material parameters that follow from the sensitivity analysis are used as input for an inverse optimization routine. In this procedure, the model is fitted to the experimental data by minimizing a least-squares objective function defined by

$$\chi^2(p) = \sum_i \left[f_{\mathrm{mod}}(x_i, p) - f_{\mathrm{exp}}(x_i)\right]^2. \quad (2)$$

In this expression, $f_{\mathrm{mod}}$ stands for the model output and $f_{\mathrm{exp}}$ the experimental output, $x_i$ represents a variable on which the output depends and over which the output is summed, and $p$ is the collection of model parameters to be determined. Surrogate modeling (Gorissen et al., 2010) was used to perform the optimization. In this technique, the parameter space defined by $p$ is initially sampled using a Maximin Latin Hypercube design to ensure maximal space filling. At the sampled points, objective function (2) is evaluated through which a surrogate model is built. Then, the minimum of the current surrogate model is determined and new samples are selected and evaluated according to the location of the current minimum. This procedure is repeated until a satisfying representation is found for the objective function and when an optimum can be identified. This optimum or minimum indicates the optimized combination of parameter values.

## 3. Results

### *3.1 Experimental results*

#### *3.1.1 Stroboscopic holography*

In Fig. 3, experimentally obtained displacement maps of the lateral TM surface are shown for S1, S2 and S3 at 1.6 kHz. The magnitude is normalized to incident pressure and the phase is taken relative to the phase of the incoming sound wave (negative phase denotes motion lagging behind sound pressure). In some cases the TM could not be fully illuminated, so that the TM displacement map is partially missing. In S3, the effect of removing the IE on TM displacements was assessed and found to be small. TM displacement maps of different samples show some differences: absolute displacements and phase patterns in S1 are different from S2 and S3, and the magnitude in S3 differs slightly from S1 and S2, having different locations of maximal displacement. In S3, a line of small displacement is apparent that corresponds to the location of the middle drum-tubal ligament (MDT, Fig. 3 - left), but it is much less prominent in other samples. Nevertheless, TM displacements evolve similarly with frequency and the number of vibration maxima differs little or not at all between samples. They are further discussed for the example of S2. In Fig. 4, the displacement maps of the lateral TM surface from S2 are shown in the first column, with selected stimulus frequencies of 0.4, 1.6 and 6.4 kHz. For all frequencies, the magnitude is smallest on the posterior part of the TM which corresponds to the attachment location of the EXC. At 0.4 kHz, the phase is uniform and the magnitude shows one area of larger displacement. At 1.6 kHz, different parts of the TM start to move out of phase with each other. These spatial transitions of the phase occur abruptly at some TM locations and continuously at others. Around 6.4 kHz, the displacement pattern becomes more complex and starts to form ring patterns around the EST.

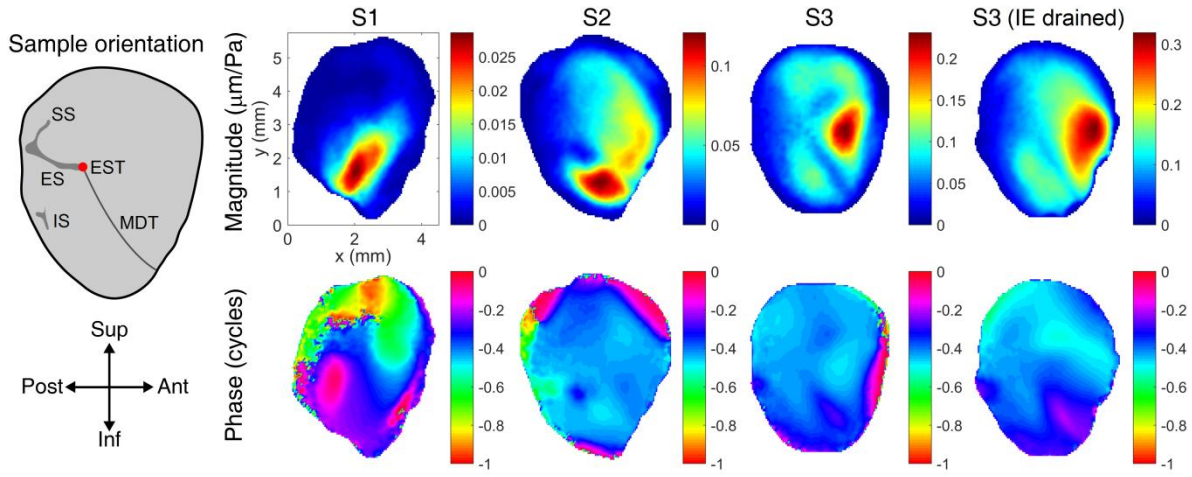


**Figure 3**. Experimental (S1, S2 and S3) displacement magnitudes (µm/Pa) and phases (cycles) of the lateral TM surface at 1.6 kHz. The last column shows TM displacements of S3 after draining the IE. Anatomical orientations and attachment

locations of the infra- (IS), extra- (ES), and suprastapedial (SS) processes are indicated. The EST is annotated by a red dot and the middle drum-tubal ligament (MDT) by a diagonal line.

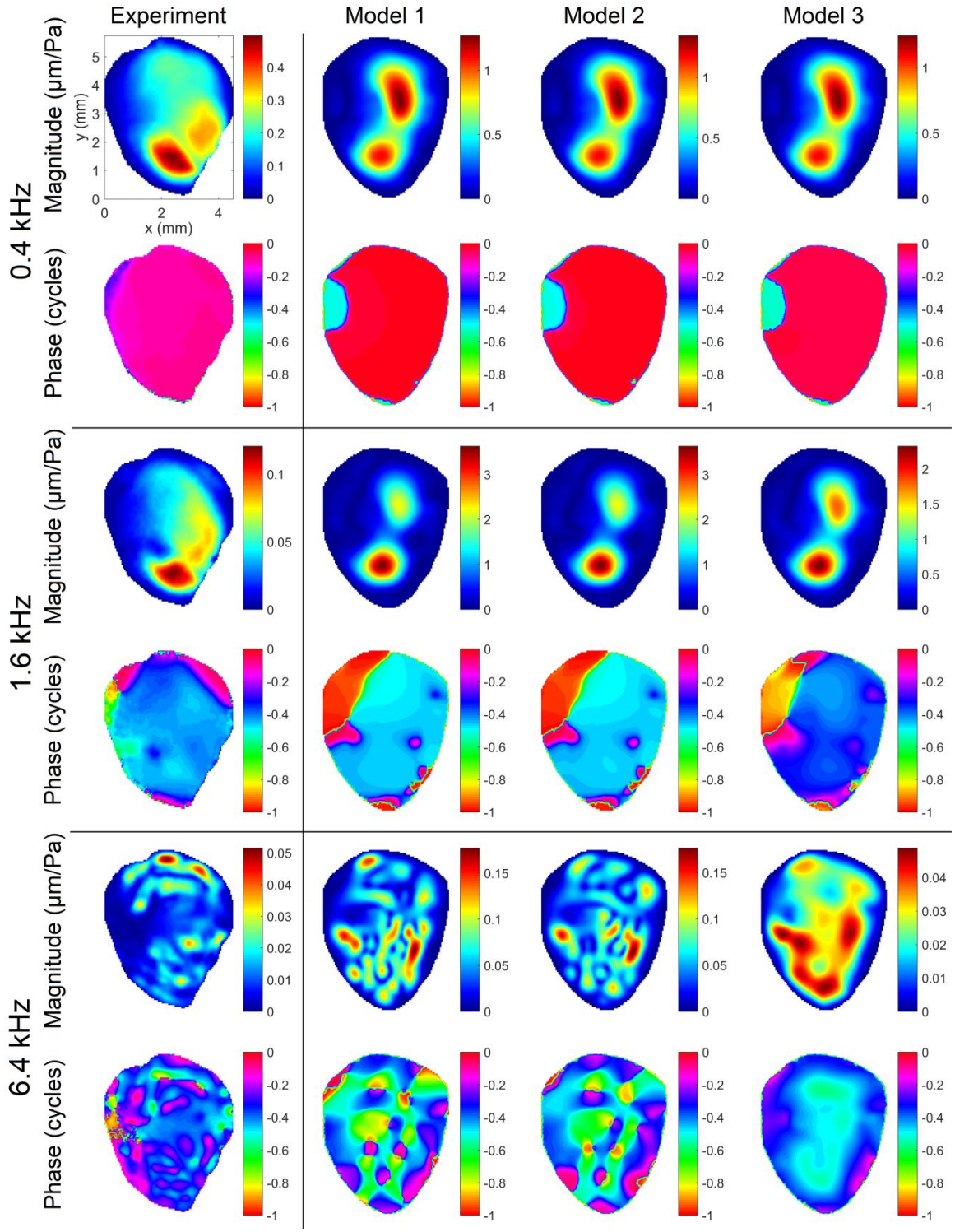


**Figure 4.** Displacement magnitudes (μm/Pa) and phases (cycles) of the lateral TM surface at 0.4, 1.6 and 6.4 kHz, for both the experiment (S2, left) and the optimized models (right). Displacement phases are taken relative to the phase of the incident pressure wave. Models are described in section 2.2.2 and 3.2.2.

### *3.1.2 Laser Doppler vibrometry*

Fig. 5 shows the vibrometry data measured on S2 (red) and S3 (blue). The top pane represents the transfer function plotted as velocity magnitude normalized to pressure, as a function of input frequency. Solid lines stand

for the response measured on the EST and dashed lines represent the FP response. All measurements were done after removal of the IE, except for the cyan colored line which shows the EST response with intact IE. The bottom pane depicts the EST-to-FP velocity ratio of S2 and S3. First we notice an offset in response between the two samples. Nevertheless, both samples show the same damped resonance near 1.5 kHz after removal of the IE. Around 6 kHz, S2 reaches a second resonance, while in S3 the response is mainly flat but higher on average. Removing the IE in S3 leaves the low-frequency response unaltered, but shifts the first resonance frequency to the right and increases the high-frequency response, which resembles the effect of removing inertial impedance from the system. In both samples, the EST-to-FP velocity ratio varies between 1.5 and 2.5 for most frequencies. The velocity ratio drops below 1 above 6 kHz (S2) and 8 kHz (S3).

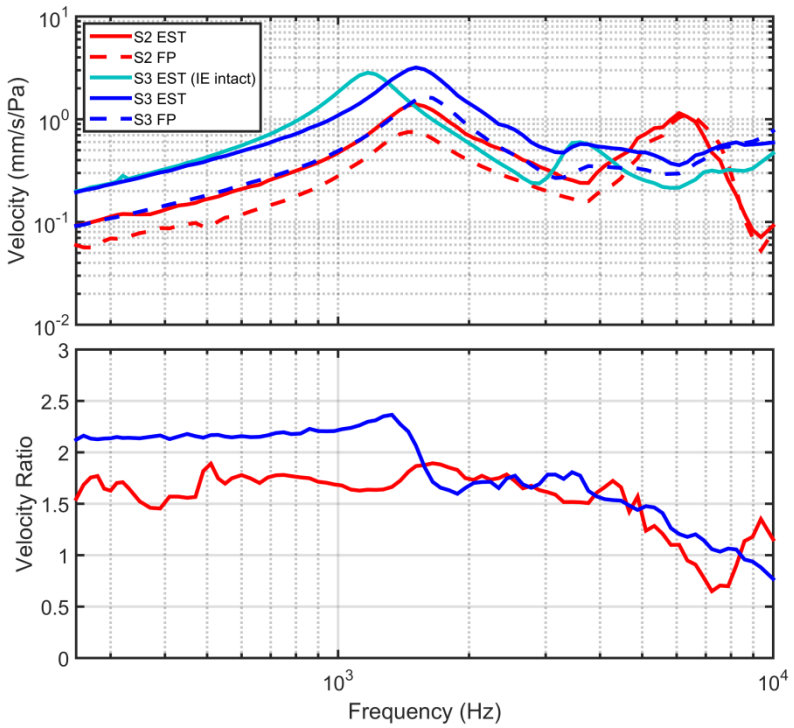


**Figure 5.** Top: Normalized velocity magnitude of the EST and FP as a function of stimulus frequency, measured on S2 and S3. Bottom: EST-to-FP velocity ratio of S2 and S3.

## *3.2 Model results*

### *3.2.1 Sensitivity analysis*

All material parameters were subject to a sensitivity analysis with the exception of the Young's modulus of Platner's ligament, because it solely serves for stabilization (Saunders et al., 2002), and all Poisson's ratios, which have been shown to be unimportant (Funnel and Laszlo, 1977). First, parameter uncertainty intervals were chosen with uniform probability distribution. If $p_0$ is the base value of each parameter (see Table 1), the lower bound $p_l$ and upper bound $p_u$ are defined as follows: $p_l = 0.1 \cdot p_0$ and $p_u = 10 \cdot p_0$ for all Young's moduli, $p_l = 0.5 \cdot p_0$ and $p_u = 1.5 \cdot p_0$ for all loss factors, and $p_l = p_0 - 100$ kg/m³ and $p_u = p_0 + 100$ kg/m³ for all mass densities. Subsequently, 400 samples were generated within the defined parameter space of the sensitivity analysis. At these samples, the full-field displacement of the TM and the EST-to-FP velocity ratio are evaluated when using model 1 at 1.6 kHz, which is near the resonance frequency (Fig. 5). Investigating the results on the TM displacement, $E_{TM}$ has the highest influence, whereas other parameters only have negligible effect and mostly contribute through interactions with $E_{TM}$. Following $E_{TM}$, $E_{EXC}$ has the second largest effect. Other material parameters, such as $\rho_{ST}$ and $\eta_{ST}$, have smaller effect given their small initial uncertainty. For the EST-to-FP velocity ratio, the influence of $E_{AL}$ is highest, followed closely by $E_{TM}$, $E_{EXC}$ and $E_C$. It is noted that most total effects of parameters are much larger than individual effects, for instance with $E_C$, which suggests that interactions between parameters and higher-order effects are very important.

### *3.2.2 Inverse analysis*

First, holography data of the TM displacement at 1.6 kHz are used as experimental input for inverse analysis. The parameter with largest influence on the TM displacement is chosen as the first parameter to determine, which turns out to be $E_{TM}$. For the second parameter we choose $E_{EXC}$ since it has the second largest effect, although we expect it to have limited influence on the overall TM displacements when compared to $E_{TM}$. For the optimization, objective function (2) is defined as

$$\chi^2(p) = \sum_i \left\{ \left[ M_{\mathrm{mod}}(\mathbf{r}_i, p) - M_{\mathrm{exp}}(\mathbf{r}_i) \right]^2 + \left[ \phi_{\mathrm{mod}}(\mathbf{r}_i, p) - \phi_{\mathrm{exp}}(\mathbf{r}_i) \right]^2 \right\}. \quad (3)$$

In this expression, $\mathbf{r}_i$ = ($x_i$, $y_i$) are the 2D TM coordinates and $p$ = ($E_{TM}$, $E_{EXC}$) are the parameters to be determined. $M$ represents the displacement magnitude and $\phi$ the phase at 1.6 kHz. $M$ and $\phi$ are both normalized to 1 in model and experiment, meaning that only displacement patterns are considered and not absolute displacements. For the TM stiffness, the objective functions for different experimental datasets reached minima at $E_{TM}$ = 41.9 MPa (S1), $E_{TM}$ = 33.0 MPa (S2) and $E_{TM}$ = 72.6 MPa (S3). For EXC stiffness, the resulting value was too uncertain to be determined precisely using any of S1, S2 or S3.

In Fig. 4, the optimized result of model 1 as obtained for S2 is compared with the experimental outcome for S2 at 0.4, 1.6 and 6.4 kHz. To study the frequency dependence of the viscoelasticity of the TM, model 2 and 3 are applied. For model 2, a pre-factor $c$ is multiplied with the frequency dependent storage modulus from De Greef et al. (2014b) such that $E_{TM}(\omega) = c \cdot E_1(\omega)$ = 33.0 MPa at 1.6 kHz. For model 3, $E_{TM}$ = 33.0 MPa and constant. Comparing the three models, similar results are obtained at 0.4 and 1.6 kHz. The models show a large area of maximal displacement on the superior part of the TM that is not seen in S2 but only in S3 (Fig. 3 - S3). Also, the model phase undergoes a sudden half-cycle jump near the EXC that is not seen in the data. At 6.4 kHz, the larger damping in model 3 at higher frequencies leads to a poorer match between the displacement patterns predicted by that model and the data. Model 1 and 2 better predict the displacement patterns; though the clearer spatial phase variations they predict are larger than those seen in the data at 6.4 kHz. Furthermore, model 1 and 2 give a better description at 6.4 kHz, even though the phase shows a little more ring patterns in the experiment. Furthermore, absolute displacements are well described at 0.4 and 6.4 kHz, only at 1.6 kHz the model displacements are one order too high.

## 4. Discussion

### *4.1 Avian ME mechanics*

In the past, the mechanics of the avian ME have been modeled as a series of mathematical equations (Relkin, 1988; Starck, 1992) and a 2D rigid-rod model (Thomassen et al., 2007) that only describe the behavior of the ME in (quasi-)static circumstances under the assumption of a priori known parameter values. Because of this scarcity of literature data, current results are also compared to existing data of mammal ME mechanics.

#### *4.1.1 Material stiffness*

The central layer of the TM in birds is composed of radial and circular collagen fibers with possibly different properties (Chin et al., 1997). In this study, the TM Young's modulus was chosen isotropic as a first approximation to not increase the number of unknown parameters. Using the holography data as experimental input for inverse analysis, the TM Young's modulus in three samples was respectively found to be 33.0, 41.9 and 72.6 MPa at 1.6 kHz. Currently, our findings can only be compared to mammals, which already show a great variety between different species, studies and specimens (e.g. Volandri et al., 2011). For instance, the values found in our study vary by a factor 2, whereas in human, fitting vibrometry measurements on two temporal bones yields a variation of a factor 4 (De Greef et al., 2014b), which clearly indicates the presence of inter-individual differences. Nevertheless, our results are within the range of what is generally found in most mammal species (~ 10 - 100 MPa). Furthermore, the sensitivity analysis shows that elasticities of the AL, EXC and columella have a large effect on the EXT-to-FP velocity ratio, which implies that their values will be needed to describe the ME transfer function and the 3D motions of the columella in future studies.

### *4.1.2 TM displacements*

As was found in human (De Greef et al., 2014b), observed TM motions suggest the presence of internal damping in the membrane: a certain amount of damping is needed to describe the continuous phase variations over the membrane at different frequencies. This amount should be small enough to allow for the complicated displacement patterns on the membrane at higher frequencies (Fig. 4), which tend to form ring patterns around the center, but it needs to be high enough to smooth out non-existing sharp resonances in the frequency dependent response of the TM, which is why absolute displacements in the vicinity of the resonance at 1.6 kHz are poorly predicted by the models. TM displacements show that a membrane with constant Young's modulus and loss factor gives almost the same results as a TM described by a third-order Maxwell model. When comparing the experimental and numerical results of displacements at low frequencies, we observe that the models show a non-existing phase jump near the EXC, which is possibly caused by not considering the ascending ligament as a separate structure. This ligament is generally found to be stiffer than the rest of the TM due to a thicker layer of collagen fibers (Chin et al., 1997).

### *4.1.3 Extrastapedial tip / footplate velocity*

First of all, the the frequency of peak velocity corresponds closely to the most sensitive frequency in mallard ducks (Trainer, Unpublished results). The velocity transfer function of the avian ME has also been measured at both the EST and FP in the ringed turtledove (*Streptopelia risoria*) (Saunders and Johnstone, 1972) and the pigeon (*Columba livia*) (Gummer et al., 1989a, 1989b). These experiments yielded peak amplitudes of 1 - 10 mm/s/Pa between 0.8 - 2 kHz, and an EST-to-FP velocity ratio of 2.2 - 2.5 between 0.125 - 4 kHz. These results are similar to our findings that denote a positive lever action, but compared to mammals (e.g. Rosowski et al., 2007; Ravicz et al., 2007) amplitudes are around ten times higher. At frequencies higher than 4 kHz, the velocity ratio was earlier found to increase above a value of 5, for which two possible explanations were suggested (Manley, 1972, 1990): either the complicated motions of the TM would significantly change displacements at the EST, or an additional flex in the extrastapedial process would absorb the TM motions. However, in our measurements, a decrease was observed above 7 kHz. Thus, an acoustic impedance mismatch at the oval window near the upper frequency limit in birds seems to take place in opposite directions for different species. Removal of the IE shifts the resonance frequency to the right in the EST velocity and increases the high frequency response. This suggests that the IE impedance is mass-dominated.

## *4.2 Method considerations*

In the optimization process of the FE model, only material parameters were considered but not the system's geometry and boundary conditions. However, it is known that for instance TM thickness has a strong influence on TM stiffness and hence the overall ME response (Aernouts et al., 2012). The same holds for the IE load, which influences motions of the columella at the EST (Fig. 5) and certainly at the FP. The reason for our choice is that each newly added parameter would drastically increase the number of required function evaluations in the sensitivity analysis and hence the total calculation time. On the other hand, sensitivities were only determined at a single frequency, while the influence of parameters can change with frequency. Nonetheless, optimization of the most influential parameters using the holography data, which was done at the same frequency as the sensitivity analysis, well predicted TM displacements at other frequencies. In each optimization, only two parameters were considered simultaneously, of which eventually only one parameter was determined. A larger number of parameters would increase the total calculation time but also the risk of over-fitting the experimental data. Even our approach has some limitations: the FE geometry is based on a different sample than the ones used in the experiments, and measurements performed on three specimens show some differences. For instance, small differences in ME geometry may cause the optimized parameters to be consistently over- or underestimated. Therefore, optimized material parameters should be taken with some caution, and because only three samples were studied, definite conclusions may not be drawn yet. Nevertheless, we expect geometrical effects to be small when compared to the inter-individual variances on the obtained material parameters themselves.

## 5. Conclusions

In this study, the acoustic response and mechanical properties of the single-ossicle ME of birds were studied for the first time by combining the results of vibrational experiments with FE simulations. From the analysis we found that TM displacements are mainly influenced by the TM Young's modulus, whereas the ME transfer function mostly depends on the Young's moduli of the annular ligament, the TM and the EXC, in that order.

Using holography measurements at 1.6 kHz, the TM Young's modulus was found equal to 33.0, 41.9 and 72.6 MPa in three samples respectively, showing a considerable inter-individual variability. Our results suggest that in birds, similar to mammals, moderate damping in the TM material properties produces better fits between predicted and measured phases of the TM motion patterns.

The velocity transfer functions of the EST and FP are around ten times higher in magnitude than what is generally found in mammals. The EST-to-FP velocity ratio is equal to 1.5 - 2.5 denoting a positive lever action, but at higher frequencies this ratio dropped corresponding to an increase in FP response relative to EST response and a loss of lever function.

## Acknowledgments

Financial support was supplied by the Research Foundation of Flanders (FWO), grant No. G049414N and 11T9316N. We would like to express our gratitude to the UGCT lab from the University of Ghent to make available the µCT scanner. We also thank John Peacock, Fred Wiese and William Deblauwe for their assistance.

## References

Aernouts, J., Aerts, J.R.M., Dirckx, J.J.J., 2012. Mechanical properties of human tympanic membrane in the quasi-static regime from in situ point indentation measurements. Hear. Res. 290 (1-2), 45-54. http://dx.doi.org/10.1016/j.heares.2012.05.001.

Arechvo, I., Zahnert, T., Bornitz, M., Neudert, M., Lasurashvili, N., Simkunaite-Rizgeliene, R., 2013. The ostrich middle ear for developing an ideal ossicular replacement prosthesis. Eur. Arch. Otorhinolaryngol. 270 (1), 37-44. http://dx.doi.org/10.1007/s00405-011-1907-1.

Buytaert, J.A.N., Goyens, J., De Greef, D., Aerts, P., Dirckx, J.J.J., 2014. Volume shrinkage of bone, brain and muscle tissue in sample preparation for micro-CT and light sheet fluorescence microscopy (LSFM). Microsc. Microanal. 20 (4), 1208-1217. http://dx.doi.org/10.1017/S1431927614001329.

Cheng, J.T., Aarnisalo, A.A., Harrington, E., del Socorro Hernandez-Montes, M., Furlong, C., Merchant, S.N., Rosowski, J.J., 2010. Motion of the surface of the human tympanic membrane measured with stroboscopic holography. Hear. Res. 263, 66-77. http://dx.doi.org/10.1016/j.heares.2009.12.024.

Cheng, J.T., Hamade, M., Merchant, S.N., Rosowski, J.J., 2013. Wave motion on the surface of the human tympanic membrane: holographic measurement and modeling analysis. J. Acoust. Soc. Am. 133 (2), 918-937. http://dx.doi.org/10.1121/1.4773263.

Chin, K., Kurian, R., Saunders, J.C., 1997. Maturation of tympanic membrane layers and collagen in the embryonic and post-hatch chick (Gallus domesticus). J. Morphol. 233 (3), 257-266. http://dx.doi.org/10.1002/(SICI)1097-4687(199709)233:3<257::AID-JMOR5>3.0.CO;2-0.

De Greef, D., Aernouts, J., Aerts, J., Cheng, J.T., Horwitz, R., Rosowski, J.J., Dirckx, J.J.J., 2014b. Viscoelastic properties of the human tympanic membrane studied with stroboscopic holography and finite element modeling. Hear. Res. 312, 69-80. http://dx.doi.org/10.1016/j.heares.2014.03.002.

De Greef, D., Soons, J.A.M., Dirckx, J.J.J., 2014a. Digital stroboscopic holography setup for deformation measurement at both quasi-static and acoustic frequencies. Int. J. Optomechatroni. 8 (4), 275-291. http://dx.doi.org/10.1080/15599612.2014.942928.

Dooling, R.J., Lohr, B., Dent, M.L., 2002. Hearing in birds and reptiles. In: Dooling, R.J., Fay, R.R., Popper, A.H. (Ed.), Comparative Hearing: Birds and Reptiles. Springer-Verlag, New York, pp. 308-359. http://dx.doi.org/10.1007/978-1-4612-1182-2_7.

Funnel, W.R.J., Laszlo, C.A., 1977. Modeling of the cat eardrum as a thin shell using the finite-element method. J. Acoust. Soc. Am. 63 (5), 1461-1467. http://dx.doi.org/10.1121/1.381892.

Gaudin, E.P., 1968. On the middle ear of birds. Acta Otolaryngol. 65, 316-326. http://dx.doi.org/10.3109/00016486809120971.

Gorissen, D., Couckuyt, I., Demeester, P., Dhaene, T., Crombecq, K., 2010. A surrogate modeling and adaptive sampling toolbox for computer based design. J. Mach. Learn. Res. 11, 2051-2055. ISSN: 1532-4435 EISSN: 1533-7928.

Gummer, A.W., Smolders, J.W.T., Klinke, R., 1989a. Mechanics of a single-ossicle ear: I. The extra-stapedius of the pigeon. Hear. Res. 39, 1-14. http://dx.doi.org/10.1016/0378-5955(89)90077-4.

Gummer, A.W., Smolders, J.W.T., Klinke, R., 1989b. Mechanics of a single-ossicle ear. II. The columella footplate of the pigeon. Hear. Res. 39, 15-26. http://dx.doi.org/10.1016/0378-5955(89)90078-6.

Homma, K., Du, Y., Shimizu, I., Puria, S., 2009. Ossicular resonance modes of the human middle ear for bone and air conduction. J. Acoust. Soc. Am. 125 (1), 968-976. http://dx.doi.org/10.1121/1.3056564.

Homma, K., Shimizu, Y., Kim, N., Du, Y., Puria, S., 2010. Effects of ear-canal pressurization on middle-ear bone- and air-conduction responses. Hear. Res. 263 (1-2), 204-215. http://dx.doi.org/10.1016/j.heares.2009.11.013.

Khaleghi, M., Lu, W., Dobrev, I., Cheng, J.T., Furlong, C., Rosowski, J.J., 2013. Digital holographic measurements of shape and three-dimensional sound-induced displacements of tympanic membrane. Opt. Eng. 52 (10), 101916. http://dx.doi.org/10.1117/1.OE.52.10.101916.

Manley, G.A., 1972. The middle ear of the tokay gecko. J. Comp. Physiol. 8l, 239-250. http://dx.doi.org/10.1007/BF00693629.

Manley, G.A., 1990. Peripheral Hearing Mechanisms in Reptiles and Birds. Springer-Verlag, New York. http://dx.doi.org/10.1007/978-3-642-83615-2.

Masschaele, B., Cnudde, V., Dierick, M., Jacobs, P., Van Hoorebeke, L., Vlassenbroeck, J., 2007. UGCT: new X-ray radiography and tomography facility. Nucl. Instr. Meth. Phys. Res. 580, 266-269. http://dx.doi.org/10.1016/j.nima.2007.05.099.

Merchant, S.N., Ravicz, M.E., Rosowski, J.J., 1996. Acoustic input impedance of the stapes and cochlea in human temporal bones. Hear. Res. 97 (1-2), 30-45. http://dx.doi.org/10.1016/S0378-5955(96)80005-0.

Mills, R., Zhang, J., 2006. Applied comparative physiology of the avian middle ear: the effect of static pressure changes in columellar ears. J. Laryngol. Otol. 120, 1005-1007. http://dx.doi.org/10.1017/S0022215106002581.

Norberg, R., 1978. Skull asymmetry, ear structure and function, and auditory localization in Tengmalm's owl, Aegolius funereus (Linne). Phil. Trans. R. Soc. 282 B, 325-410. http://dx.doi.org/10.1098/rstb.1978.0014.

Oakley, J., O'Hagan, A., 2004. Probabilistic sensitivity analysis of complex models: a Bayesian approach. J. R. Stat. Soc. Series B. Stat. Methodol. 66, 751-769. http://dx.doi.org/10.1111/j.1467-9868.2004.05304.x.

Pohlman, A.G., 1921. The position and functional interpretation of the elastic ligaments in the middle-ear of Gallus. J. Morphol. 35, 229-262. http://dx.doi.org/10.1002/jmor.1050350106.

Ravicz, M.E., Cooper, N.P., Rosowski, J.J., 2007. Gerbil middle-ear sound transmission from 100 Hz to 60 kHz. J. Acoust. Soc. Am. 124 (1), 363-380. http://dx.doi.org/10.1121/1.2932061.

Rosowski, J.J., Chien, W., Ravicz, M.E., Merchant, S.N., 2007. Testing a method for quantifying the output of implantable middle ear hearing devices. Audiol. Neurootol. 12 (4), 265-276. http://dx.doi.org/10.1159/000101474.

Relkin, E.M., 1988. Introduction to the analysis of middle-ear function. In: Jahn, A.F., Santos-Sacchi, J. (Eds.), Physiology of the Ear. Raven Press, New York, pp. 103-123. ISBN: 1565939948, ISBN13: 9781565939943.

Saunders, J.C., Duncan, R.K., Doan, D.E., Werner, Y.L., 2002. The middle ear of reptiles and birds. In: Dooling, R.J., Fay, R.R., Popper, A.H. (Ed.), Comparative Hearing: Birds and Reptiles. Springer-Verlag, New York, pp. 13-69. http://dx.doi.org/10.1007/978-1-4612-1182-2_2.

Saunders, J.C., Johnstone, B.M., 1972. A comparative analysis of middle-ear function in non-mammalian vertebrates. Acta. Otolaryngol. 73, 353-361. http://dx.doi.org/10.3109/00016487209138952.

Spahn, G., Wittig, R., 2003. Biomechanical properties (compressive strength and compressive pressure at break) of hyaline cartilage under axial load. Zentralbl. Chir. 128, 78-82. http://dx.doi.org/10.1055/s-2003-37325.

Starck, J.M., 1992. Towards a model of the functional morphology of the avian middle ear - The transfer function. Zool. Jahrb. Anat. 122, 287-302. ISSN: 0044-5177.

Starck, J.M., 1995. Comparative anatomy of the external and middle ear of palaeognathous birds. Adv. Anat. Embryol. Cell Biol. 131, 1-137. http://dx.doi.org/10.1007/978-3-642-79592-3.

Thomassen, H.A., Gea, S., Maas, S., Bout, R.G., Dirckx, J.J.J., Decraemer, W.H., Povel, G.D.E., 2007. Do Swiftlets have an ear for echolocation? The functional morphology of Swiftlet's middle ears. Hear. Res. 225, 25-37. http://dx.doi.org/10.1016/j.heares.2006.11.013.

Trainer, J. E., Unpublished results. The auditory acuity of certain birds. Ph.D. thesis, Cornell University, Ithaca, New York, USA.

Van der Jeught, S., Dirckx, J.J.J., Aerts, J.R.M., Bradu, A., Podoleanu, A.G., Buytaert, J.A.N., 2013. Full-field thickness distribution of human tympanic membrane obtained with optical coherence tomography. J. Assoc. Res. Otolaryngol. 14 (4), 483-493. http://dx.doi.org/10.1007/s10162-013-0394-z.

Volandri, G., Di Puccio, F., Forte, P., Carmignani, C., 2011. Biomechanics of the tympanic membrane. J. Biomech. 44 (7), 1219-1236. http://dx.doi.org/10.1016/j.jbiomech.2010.12.023.

Zhang, X., Gan, R.Z., 2010. Dynamic properties of human tympanic membrane - experimental measurement and modeling analysis. Int. J. Exp. Comput. Biomech. 1, 252-270. http://dx.doi.org/10.1186/2193-1801-2-527.